A toroidal metamaterial switch

Gupta, Manoj; Srivastava, Yogesh Kumar; Singh, Ranjan

2018

Gupta, M., Srivastava, Y. K., & Singh, R. (2018). A Toroidal Metamaterial Switch. Advanced Materials, 30(4), 1704845-. doi:10.1002/adma.201704845

https://hdl.handle.net/10356/88518

https://doi.org/10.1002/adma.201704845

Article type: Communication

A Toroidal Metamaterial Switch

*Manoj Gupta, Yogesh Kumar Srivastava, and Ranjan Singh**

M. Gupta, Y. K. Srivastava, Prof. R. Singh
Division of Physics and Applied Physics, School of Physical and Mathematical Sciences, Nanyang Technological University, Singapore 637371, Singapore

Centre for Disruptive Photonic Technologies, The Photonics Institute, Nanyang Technological University, Singapore 637371, Singapore

E-mail: ranjans@ntu.edu.sg

Keywords: Toroidal dipole, Electric dipole, Magnetic dipole, Anapole

Abstract:

Toroidal dipole is a localized electromagnetic excitation that plays an important role in determining the fundamental properties of matter due to its unique potential to excite nearly non-radiating charge-current configuration. Toroidal dipoles were recently discovered in metamaterial systems where it has been shown that these dipoles manifest as poloidal currents on the surface of a torus and are distinctly different from the traditional electric and magnetic dipoles. Here, we demonstrate an active toroidal metamaterial switch in which the toroidal dipole could be dynamically switched to the fundamental electric dipole or magnetic dipole, through selective inclusion of active elements in a hybrid metamolecule design. Active switching of non-radiating toroidal configuration into highly radiating electric and magnetic dipoles can have significant impact in controlling the electromagnetic excitations in free space and matter that could have potential applications in designing efficient lasers, sensors, filters, and modulators.

Introduction:

Subwavelength metallic resonators provides an innovative approach to manipulate the electromagnetic response of macroscopic media.[1-15] The electromagnetic response originating from the individual subwavelength photonics resonators is due to induced charge/current distribution, which are further categorized in terms of electric, magnetic and toroidal multipoles.[16,17] Here, the nature of individual multipole signifies the extent of coupling to free space, which plays an important role in tailoring the losses by radiative means.[18, 19] In the burgeoning field of metamaterials, a well-established framework has been developed to play around the loss channels influenced by the electric and magnetic responses,[20,21] but recently there has been intense interest in toroidal electrodynamics for loss engineering.[22] Toroidal dipole is visualized as the currents flowing on the surface of torus (poloidal currents) along its meridians, where array of magnetic dipoles originating from poloidal currents are arranged in head-to-tail configuration along a torus. In metamaterials, several works discussed novel schemes that mimic the 3D torus configuration for the electromagnetic excitation of the toroidal dipole.[23,24] However, the electromagnetic response of artificial media with toroidal topology is also accompanied by electric and magnetic multipoles. The flexibility in tailoring the moment of toroidal dipole allows to explore one of the exotic feature in terms of non-radiating charge current configuration, commonly known as anapole, due to destructive interference of electric and toroidal dipole.[25-27] Recently, an idea of anapole-based nanolasers have been proposed, where stimulated emission amplifies an anapole mode in dielectric resonator.[28] Though, it is very difficult to achieve perfect anapole conditions, yet researches are more focused towards the toroidal dipole mode because it offers weak electromagnetic scattering compared to the electric and magnetic dipoles, and could lower the radiative loss due to electric dipole, which is dominant in almost all kinds of electromagnetically excited metasurfaces. In three-dimensional artificial media, the dynamic toroidal moment were exploited to observe well known electromagnetic phenomena such as resonant transparency and circular dichroism.[29,30] Even in 2D metasurfaces, introduction of

toroidal coupling enhances device performance in terms of quality facor (Q), which is defined as the ratio of resonance frequency to the full width at half maximum, and figure of merit (FoM $= Q \times \Delta I$, product of the Q-factor and the resonance intensity (ΔI)) of the electromagnetic resonance.[31-36]

Line-width of an electromagnetic resonance depends on the nature and strength of the scattering phenomenon. Depending upon the excitation requirements, the electromagnetic response of the metamaterial array can be of electric, magnetic or toroidal type, which is achieved by passively modifying the unit cell configuration. For instance, electric dipole that scatters strongly due to their broad line-width, are used as antenna or local sensors to probe the near field.[37] Similarly, magnetic dipole, which has comparatively narrower line-width, is used as dielectric/strain sensor and most importantly in the excitation of the toroidal dipole.[38,39] Switching electromagnetic response between these characteristic dipoles will necessarily provide a promising route towards building new optical devices. Moreover, active tuning of toroidal excitation will definitely add other key functionalities to metamaterial based devices, which are important for potential applications.

Here, we demonstrate a metamaterial toroidal switch that could dynamically transition from nearly non-radiative *toroidal configuration to electric or magnetic dipole excitations*. In this active scheme, an ultrathin silicon layer beneath the capacitive split gap of a metallic resonator in the unit cell of metamaterial array acts as a dynamic material that precisely controls the optical properties of the hybrid metamaterial with the help of external stimulus in the form of near infrared femtosecond pulses. The unit cell design consists of a planar asymmetric resonator pair arranged in the mirrored configuration, which supports a toroidal resonance excitation. By judiciously suppressing electromagnetic resonance of one or both resonators in mirrored configuration, one can dynamically switch from toroidal resonance to a magnetic dipole or an electric dipole resonance. Our result also manifests smooth transition and complete modulation of toroidal resonance at very low pump fluence. For toroidal to

electric dipole transition, the experimentally achieved maximum value of peak to peak amplitude modulation depth is 73%, which is defined as $(T_{off}-T_{on})/T_{off} \times 100$ for the entire spectral range, where T_{off} and T_{on}, respectively, stands for the transmission amplitudes during 'off' and 'on' stage of optical pump. We also obtained a point (in frequency) of nearly constant intensity transmission during the course of active tuning across a broad spectral range.

Discussion:

The active control mechanism of toroidal resonances is enabled by a hybrid metasurface containing silicon pads at the split gaps of terahertz split ring resonator structure. **Figure 1a** shows the microscopic image of the fabricated sample along XY plane, where the zoomed unit cell reveals the mirrored configuration of terahertz asymmetric split ring resonators (TASRs). The outer dimension of individual resonator is 60 µm × 60 µm, with arm width of 6 µm and the split-gap size equal to 3 µm. The asymmetric nature of the TASR structure is due to positioning of both the split gaps, which are located 10 µm away from the centre of the resonator. The unit cell has periodicity of 150 µm × 75 µm in which mirrored TASRs are separated by a distance of 15 µm. The enlarged image of unit cell displays rectangular patches of silicon beneath the split gaps of the mirrored resonator, which upon photoexcitation generate free carriers that enables the active control of the toroidal response. The metamaterial samples were fabricated using two step lithography cycle followed by reactive ion etching (RIE). The metallic resonators are fabricated by thermally depositing 200 nm thick aluminium (Al) on silicon on sapphire (SoS) substrate composed of 600 nm thick silicon epilayer and 460 µm thick sapphire. RIE results in removal of undesired silicon from the structure, such that silicon remains beneath the metallic strip and at the split gaps of TASRs. In the absence of pump beam, THz excitation of *mirrored* TASRs with incident electric field

polarization along X-direction ($\vec{E}_x$) (as shown in Figure 1b), results in excitation of both symmetric dipole mode (bright mode) at higher frequency and anti-symmetric toroidal dipole resonance mode (the dark mode) at lower frequency. In the state of toroidal dipole resonance, induced circulating oscillatory currents in mirrored configuration are opposite in nature (see image labelled as 'Toroidal Dipole' in Figure 1b). Such a current distribution leads to tightly confined loops of oscillating magnetic field ($\vec{H}$) that curl around the fictitious arrow, which is a characteristic feature of the toroidal dipole vector ($\vec{T}$) in 3D space. As the pump beam illuminates the metasurface, photo excitation of silicon pads increase its conductivity that gradually alters the nature and strength of the toroidal resonances. At higher pump fluences, depending on the placement of silicon pads in split gaps of one or both TASRs, the excited current distribution, as shown by Figure 1b, either switches to anti-symmetric magnetic dipole (dark mode) or purely symmetric electric dipole (bright mode) configuration.

Optical-pump and THz-probe (OPTP) spectroscopy has been used for the optical characterization of hybrid silicon TASR samples, wherein pulsed optical beam of 800 nm wavelength is incident for photoexcitation of metamaterial sample and the photo-response of excited metasurface is probed by shining THz pulse at normal incidence with a beam diameter of 3 mm. Amplified pulsed laser of pulse width 120 fs and repetition rate of 1 kHz respectively, has been used as the pump beam. Pump beam with beam diameter of 10 mm has been employed to ensure uniform photoexcitation excitation in the vicinity of THz-probe beam interaction with metasurface. With respect to every pump pulse, THz pulse is delayed by 12 picoseconds to capture the excitation phenomenon at a particular instant, when the free carrier density in photo-excited silicon layer is maximum.

Photo-active mediated switching of toroidal resonance has been realized here by illuminating fabricated sample at different pump fluence, which is defined as radiant energy received per unit surface area ($\mu J/cm^2$). **Figure 2a** shows the experimental results depicting transmitted

intensity response with increasing fluence of pump beam. In the absence of pump illumination, with incident THz beam polarized along the X-direction (E_x), the anti-symmetric toroidal dipole resonance mode first appears at frequency of 0.453 THz and symmetric electric dipole mode appears at frequency 0.82 THz. Since, the chosen scheme provides the freedom to tailor the anti-symmetric mode (the dark mode), we focused our discussion on the lower frequency toroidal resonance.With gradual increase in the pump power, the amplitude of toroidal resonance decreases, while no significant change is recorded in the broad symmetric mode. At increased pump powers, silicon which is primarily a semiconductor starts behaving like a quasi-metal due to large photocarrier generation. This change in behaviour of silicon conductivity shorts the capacitive split-gaps of TASR pair in the unit cell, which leads to complete disappearance of the toroidal resonance feature of the metasurface for higher pump powers beyond 50 mW (pump fluence of 63.6 μJ/cm^2). The only resonance that survives in the transmittance spectra is that of an electric dipole. For the estimation of normalized transmittance at different values of pump powers, measurements have been performed by alternatively scanning THz pulse through the fabricated photo-excited metamaterial sample and bare sapphire substrate which acts as the reference. The intriguing feature that we observed at different pump powers, is the point of near constant transmission at the frequency of 0.486 THz as shown by the dotted line in Figure 2a (see supporting information for transmittance spectra at other pump powers). The signature of constant transmission point arises due to near perfect destructive interference between the sharp dark mode (toroidal) and bright mode (dipole) close to the frequency where the toroidal resonance originates. In the present metamaterial structure, a strong anti-symmetric dark toroidal resonance mode leads to the observation of the near constant transmission. Such observations are rare due to typical weak excitations of dark mode resonances in most metamaterial and plasmonic systems. To study the photo-active tuning of the toroidal resonances, we employed numerical simulation using a commercially available CST Microwave Studio frequency domain solver, based on

finite integration method. During numerical simulations TASRs have been modelled as lossy Aluminium metal with DC conductivity (σ_{DC}) of 3.56×10^7 S/m , sapphire ($\varepsilon_r = 11.7$) as a transparent substrate, and silicon ($\varepsilon_r = 11.9$) layer sandwiched between aluminium and sapphire. In simulations, the conductivity of Si has been modelled using experimentally extracted photoconductivity of the unpatterned 600 nm silicon epitaxial layer on sapphire (SOS) for the corresponding fluence of the excitation pulse. Figure 2b shows the simulated normalized transmittance spectra of silicon implanted TASRs for the increasing conductivity (σ_{Si}) of silicon layer. $\sigma_{Si} = 0$ curve corresponds to a situation when there is no illumination of metasurface by the pump beam. As σ_{Si} increases, the amplitude of toroidal resonance decreases and the resonance almost disappears at $\sigma_{Si} = 4000$ S/m. In the absence of the pump illumination, the anti-symmetric toroidal mode dominates the overall response at the lower frequency. When the pump beam is switched on, the dark anti-symmetric toroidal mode completely switches off at larger pump fluences and the purely symmetric electric dipole mode is observed at 0.68 THz (Figure 2b). The symmetric bright mode always exist in the transmission spectra. We actively switch the metamaterial from the two resonance state (toroidal + dipole) to a single resonant state which is a pure symmetric electric dipole. When the capacitive split gaps are shorted due to the large photoconductivity of silicon pads upon photoexcitation, the metamaterial structure becomes a perfect symmetrical structure that supports only a bright, broad linewidth electric dipole resonance. Therefore, through optical pumping weakly radiating toroidal mode has been switched to a strongly radiating electric dipolar mode due to the shorting of the capacitive gaps of TASRs. Also, the minute red shift (shown by dotted arrow in Figure 2a, 2b) in the frequency of toroidal resonance, because of optical pumping, in experimental as well as in simulated results can be explained by an analogous inductive-capacitive (LC) circuit model with resonance frequency

(f_{reso}) expression $f_{reso} = \frac{1}{2\pi C R_{Si}} \sqrt{\frac{C R_{Si}^2}{L} - 1}$, where R_{Si} is shunt resistance of optically pumped silicon pad, L is the inductance of TASR and C is the split-gap capacitance of TASR (see supporting information for more details). At higher values of pump fluences, the low amplitude toroidal resonance nearly disappears, so the measurement of the red shift in the toroidal resonance becomes difficult.

Furthermore, we carried out multipole analysis to investigate the role of near field toroidal coupling for different transmittance curves, and to establish the fact that modulation of the anti-symmetric toroidal mode (at lower frequency) can be achieved by tailoring the conductivity of split-gaps of the TASRs in the unit cell.[40] Here, it is important to mention that our analysis is limited to toroidal coupling between the TASR pair that forms the unit cell. **Figure 3** shows transmitted intensity (inset plot) and corresponding toroidal component ($\boldsymbol{T_x}$) computed through multipole analysis. Transmitted intensity (inset plot) computed through multipole analysis shows similar trend as experiments, which validates the modelling of the metamaterial array via multipole analysis. The peak of toroidal moment for $\sigma_{Si} = 0$ corresponds to the strength of coupling between the two mirrored resonators in the absence of pump pulse. With an increase in the intensity of the photoexcitation, σ_{Si} increases, which leads to the reduction in the strength of toroidal coupling from $\sigma_{Si} = 100$ to 4000 S/m. This deterioration in toroidal coupling results in the broadening of resonance line-width as well as decrease in the amplitude of resonance (as shown in Figure 2 and in inset of Figure 3). Besides active tuning, we obtained a smooth transition of toroidal resonance trough and transmission peak, between the on-off positions of pump fluences. In terms of modulation depth, **Figure 4** depicts percentage variation in experimentally measured transmission amplitude at different values of pump fluences for the entire range of frequency spectrum. The change in amplitude is significantly large at the resonant transmission peak (0.545 THz)

compared to that of resonance dip at 0.453 THz. Experimentally achieved peak to peak amplitude modulation depth between toroidal resonance trough (region shaded in blue) and the associated transmission peak (region shaded in grey) is about 73%. Pump powers involved in the current scheme is reasonably low compared to the schemes reported previously in the literature for switching electromagnetic resonances in the THz regime.

In continuation, we also numerically examined the situation, where electromagnetic response of mirrored TASR configuration is switched between toroidal dipole (anti-parallel magnetic dipoles) to parallel magnetic dipole type excitation. **Figure 5** shows the simulated amplitude transmission versus frequency spectra of the metasurface having Si pads below the split gaps of only one TASR in mirrored arrangement. As the conductivity of Si increases, the amplitude of toroidal dipole resonance decreases until we reach a σ_{Si} value of 1200 S/m. Increasing the silicon conductivity beyond this point excites new mode in form of parallel magnetic dipoles. The evolution of new resonance mode is at different frequency (~ 0.4 THz) from the frequency of toroidal resonance (~ 0.415 THz). At the two different conductivities of silicon (σ_{Si} = 0 and 8000 S/m), **Figure 6** shows relative induced moments of electric dipole (P_x), and toroidal dipole (T_x) along the X-direction and the magnetic dipole (M_z) along the Z-direction. Multipole calculations reveals a strong enhancement (more than two orders of magnitude) in strength of magnetic dipole (M_z), as toroidal resonance (grey region) switches to magnetic resonance (green region). To get clear idea about switching the simulated surface currents at resonance for the two different conductivities of silicon are depicted in **Figure 7a, b**, where $\vec{m}$ (magnetic dipole vector) corresponds to loop current of individual TASR in mirrored configuration. At $\sigma_{Si} = 0$ (see Figure 7a) the strong excitation of both TASRs corresponds to toroidal dipole (anti-parallel magnetic dipoles). With increase in conductivity, one of the TASR with photo-excited silicon pads quenches the magnetic moment resonance at lower frequency (~ 0.4 THz)(see Figure 7b), which eliminates toroidal coupling between the TASR

pair and the only strong excitation is due to one TASR (without silicon pads), which is of magnetic dipole type. In fact, under the influence of strongly excited resonator (without silicon pads), TASR with silicon pads carries identical current distribution, but of very weak strength, thus having its $\vec{m}$ vector identical to strongly excited TASR. This makes the whole array resemble a magnetic dipole oriented in the same direction. To differentiate this scheme from the one with the fabricated sample, where silicon pads are present in gaps of the mirrored TASR pair during the 'off'(Figure 7c) and 'on'(Figure 7d) instance of pump beam, where the nature of currents in individual TASR switches from antiparallel to parallel (electric dipole excitation) behaviour. At this instant, the toroidal cavity fails to store electromagnetic energy which lowers the amplitude of resonance (see supporting information for *Q*-factor and FoM details) compared to a situation when there is no pump illumination. Switching between the different types of dipoles can be further understood by the simulated results for electric/magnetic field distribution in **Figure 8**. Figure 8a, b, c shows electric energy confined in the splits gaps of mirrored resonators as toroidal dipole switches to electric or magnetic dipole. Energy confined is maximun for the toroidal dipole and minimum for the electric dipole. Further, as the nature of electromagnetic response switches from toroidal to magnetic, the magnetic field concentration along the Z-direction (perpendicular to the plane of array), as shown by Figure 8d and Figure 8f, also switches from antisymmetric (+Z, -Z) to symmetric(+Z, +Z) for mirrored TASR pair. Thus, depending upon the selective location of the silicon pads in split gaps of mirrored TASRs, one can tailor the nature of electromagnetic radiation from a toroidal form to either a magnetic or an electric dipole.

Conclusion:

In summary, electromagnetic excitation of multipoles is a useful tool to capture the inherent properties of electromagnetically active media. Actively controlled electromagnetic features of various multipoles, ranging from non-radiating to strongly radiating, in one device would

certainly have a key role in designing resonance-based sensing, lasing and ultrafast switching devices. We have demonstrated the dynamic switching of toroidal response to the fundamental electric or magnetic response in a single metamaterial device, through selective inclusion of active elements in a hybrid metamolecule design. We also recorded significantly high peak to peak amplitude modulation of 73% as electromagnetic resonance switches from toroidal to electric dipole. Our approach provides a new and promising method for designing novel toroidal resonance based active devices and narrow band active filters at the terahertz frequency regime.

Acknowledgements:
This work was supported by Singapore Ministry of Education Grant No. MOE2015-T2-2-103.

References:

[1] J. B. Pendry, A. J. Holden, D. J. Robbins, W. J. Stewart, *IEEE Trans. Microwave Theory Tech.* **1999**, *47*, 2075.

[2] D. R. Smith, J. B. Pendry, M. C. K. Wiltshire, *Science* **2004**, *305*, 788.

[3] J. B. Pendry, *Phys. Rev. Lett.* **2000**, *85*, 3966.

[4] T. J. Yen, W. J. Padilla, N. Fang, D. C. Vier, D. R. Smith, J. B. Pendry, D. N. Basov, X. Zhang, *Science* **2004**, *303*, 1494.

[5] A. N. Grigorenko, A. K. Geim, H. F. Gleeson, Y. Zhang, A. A. Firsov, I. Y. Khrushchev, J. Petrovic, *Nature* **2005**, *438*, 335.

[6] M. Manjappa, Y. K. Srivastava, A. Solanki, A. Kumar, T. C. Sum, R. Singh, *Adv. Mater.* **2017**, *29*, 1605881.

[7] X. Zhang, Z. Liu, *Nat. Mater.* **2008**, *7*, 435.

[8] G. Rosenblatt, M. Orenstein, *Phys. Rev. Lett.* **2015**, *115*, 195504.

[9] T. T. Lv, Y. X. Li, H. F. Ma, Z. Zhu, Z. P. Li, C. Y. Guan, J. H. Shi, H. Zhang, T. J. Cui, *Sci. Rep.* **2016**, *6*, 23186.

[10] L. Liu, L. Kang, T. S. Mayer, D. H. Werner, *Nat. Commun.* **2016**, *7*, 13236.

[11] M. V. Cojocari, K. I. Schegoleva, A. A. Basharin, *Opt. Lett.* **2017**, *42*, 1700.

[12] N. I. Zheludev, S. L. Prosvirnin, N. Papasimakis, V. A. Fedotov, *Nat. Photonics* **2008**, *2*, 351.

[13] Y.-W. Huang, W. T. Chen, P. C. Wu, V. A. Fedotov, N. I. Zheludev, D. P. Tsai, *Sci. Rep.* **2013**, *3*, 1237.

[14] J. B. Pendry, D. Schurig, D. R. Smith, *Science* **2006**, *312*, 1780.

[15] D. Schurig, J. J. Mock, B. J. Justice, S. A. Cummer, J. B. Pendry, A. F. Starr, D. R. Smith, *Science* **2006**, *314*, 977.

[16] J. Petschulat, C. Menzel, A. Chipouline, C. Rockstuhl, A. Tünnermann, F. Lederer, T. Pertsch, *Phys. Rev. A* **2008**, *78*, 043811.

[17] K. Marinov, A. D. Boardman, V. A. Fedotov, N. Zheludev, New J. Phys. **2007**, *9*, 324.

[18] G. N. Afanasiev, Yu. P. Stepanovsky, *J. phys. A. Math. Gen.* **1995**, *28*, 4565.

[19] E. E. Radescu, G. Vaman, *Phys. Rev. E* **2002**, *65*, 046609.

[20] D. Ö. Güney, T. Koschny, C. M. Soukoulis, *Phys. Rev. B* **2009**, *80*, 125129.

[21] B. Luk'yanchuk, N. I. Zheludev, S. A. Maier, N. J. Halas, P. Nordlander, H. Giessen, C. T. Chong, *Nat. Mater.* **2010**, *9*, 707.

[22] N. Papasimakis, V. A. Fedotov, V. Savinov, T. A. Raybould, N. I. Zheludev, *Nat. Mater.* **2016**, *15*, 263.

[23] T. Kaelberer, V. A. Fedotov, N. Papasimakis, D. P. Tsai, N. I. Zheludev, *Science* **2010**, *330*, 1510.

[24] Z. Liu, S. Du, A. Cui, Z. Li, Y. Fan, S. Chen, W. Li, J. Li, C. Gu, *Adv. Mater.* **2017**, *29*, 1606298.

[25] A. E. Miroshnichenko, A. B. Evlyukhin, Y. F. Yu, R. M. Bakker, A. Chipouline, A. I. Kuznetsov, B. Luk'yanchuk, B. N. Chichkov, Y. S. Kivshar, *Nat. Commun.* **2015**, *6*, 8069.

[26] A. A. Basharin, V. Chuguevsky, N. Volsky, M. Kafesaki, E. N. Economou, *Phys. Rev. B* **2017**, *95*, 035104.

[27] N. A. Nemkov, I. V. Stenishchev, A. A. Basharin, *Sci. Rep.* **2017***, 7,* 1064.

[28] J. S. T. Gongora, A. E. Miroshnichenko, Y. S. Kivshar, A. Fratalocchi, *Nat. Commun.* **2017**, *8*, 15535.

[29] V. A. Fedotov, A. V. Rogacheva, V. Savinov, D. P. Tsai, N. I. Zheludev, *Sci. Rep.* **2013**, *3*, 2967.

[30] T. A. Raybould, V. A. Fedotov, N. Papasimakis, I. Kuprov, I. J. Youngs, W. T. Chen, D. P. Tsai, N. I. Zheludev, *Phys. Rev. B*, **2016**, *94*, 035119.

[31] M. Gupta, R. Singh, *Adv. Opt. Mater.* **2016**, *4*, 2119.

[32] X. Chen, W. Fan, *Opt. Lett.* **2017**, *42*, 2034.

[33] Y. Fan, Z. Wei, H. Li, H. Chen, C. M. Soukoulis, *Phys. Rev. B* **2013**, *87*, 115417.

[34] M. Gupta, V. Savinov, N. Xu, L. Cong, G. Dayal, S. Wang, W. Zhang, N. I. Zheludev, R. Singh, *Adv. Mater.* **2016**, *28*, 8206.

[35] L. Cong, Y. K. Srivastava, R. Singh, *Appl. Phys. Lett.* **2017**, *111*, 081108.

[36] S. Han, M. Gupta, L. Cong, Y. K. Srivastava, R. Singh, *J. Appl. Phys.* **2017**, *122*, 113105.

[37] B. Metzger, M. Hentschel, H. Giessen, *Nano Lett.* **2017**, *17*, 1931.

[38] H. Tao, L. R. Chieffo, M. A. Brenckle, S. M. Siebert, M. Liu, A. C. Strikwerda, K. Fan, D. L. Kaplan, X. Zhang, R. D. Averitt, F. G. Omenetto, *Adv. Mater.* **2011**, *23*, 3197.

[39] G. Ekinci, A. D. Yalcinkaya, G. Dundar, H. Torun, presented at *27th Micromechanics and Microsystems Europe Workshop*, Cork, Ireland, August, **2016**.

[40] V. Savinov, V. A. Fedotov, N. I. Zheludev, *Phys. Rev. B* **2014**, *89*, 205112.

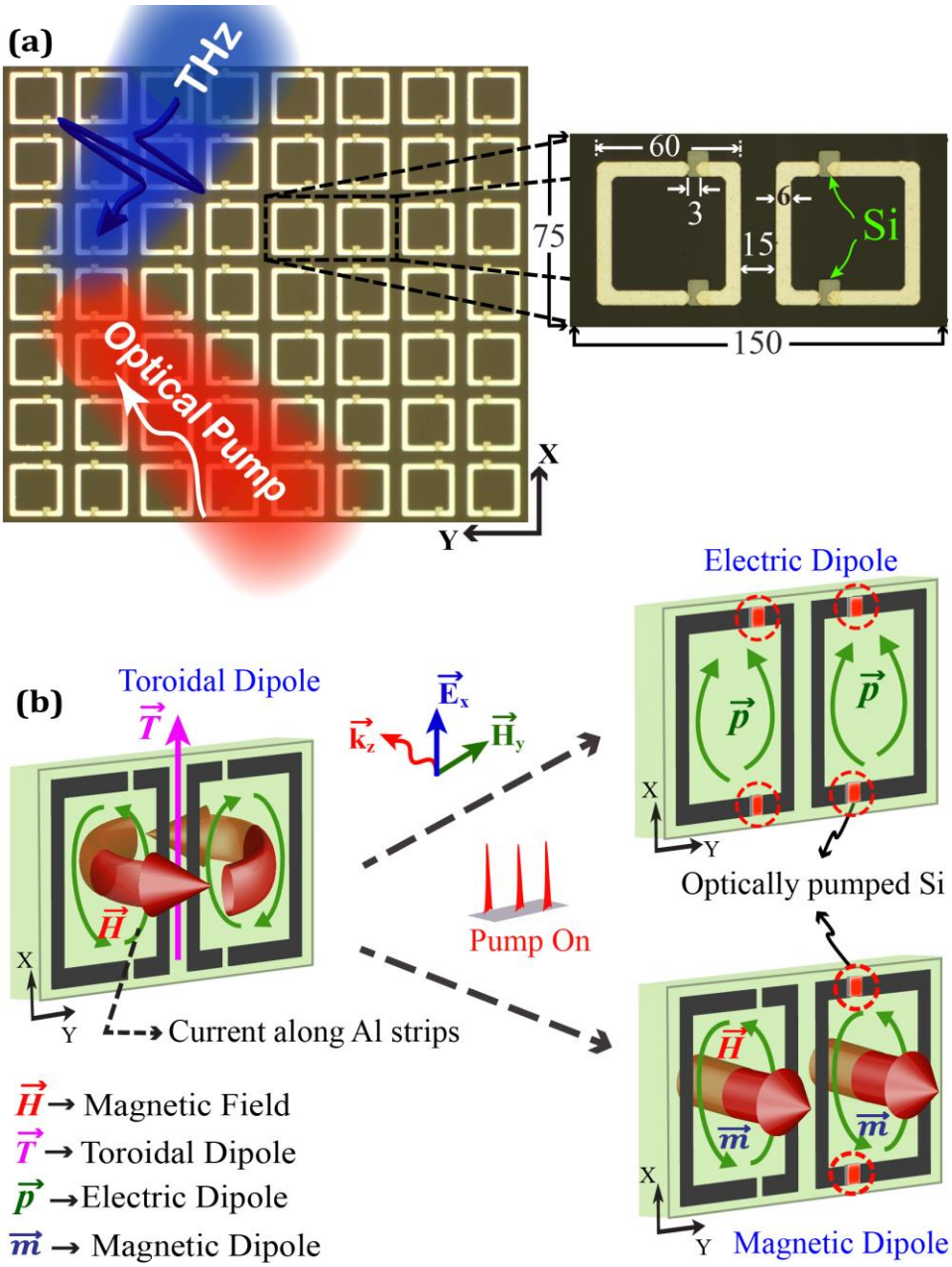

Figure 1. (a) Microscopic image of fabricated metamaterial sample, along the XY plane, illuminated with pump beam in presence of THz pulse, where zoomed image shows unit cell dimensions (in microns) of Si implanted TASRs arranged in mirrored configuration, (b) Switching in the response of unit cell from toroidal dipole to electric or magnetic dipole in presence of optical pump.

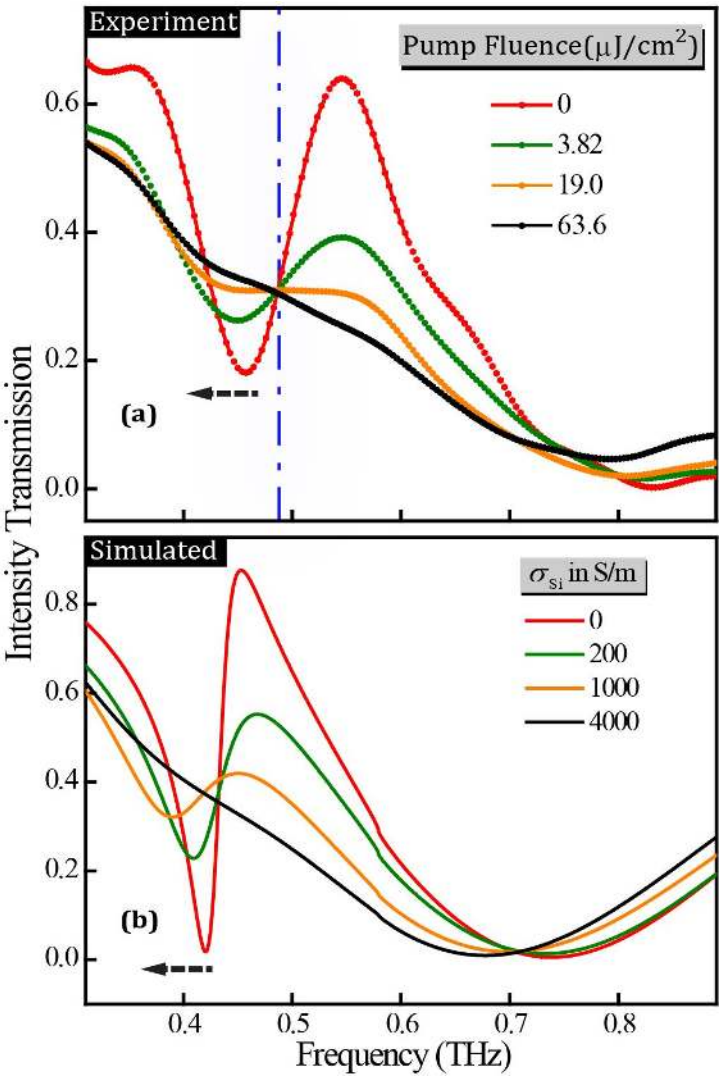

Figure 2. Transmitted intensity spectra of toroidal metasurface at different pump fluences for experimental (a) and at the corresponding conductivities for simulated (b) results, when electric field is polarized perpendicular to the gap arm of TASR. The dotted line shows the point of nearly constant transmission. Dotted arrow shows minute red shift in frequency of toroidal resonance.

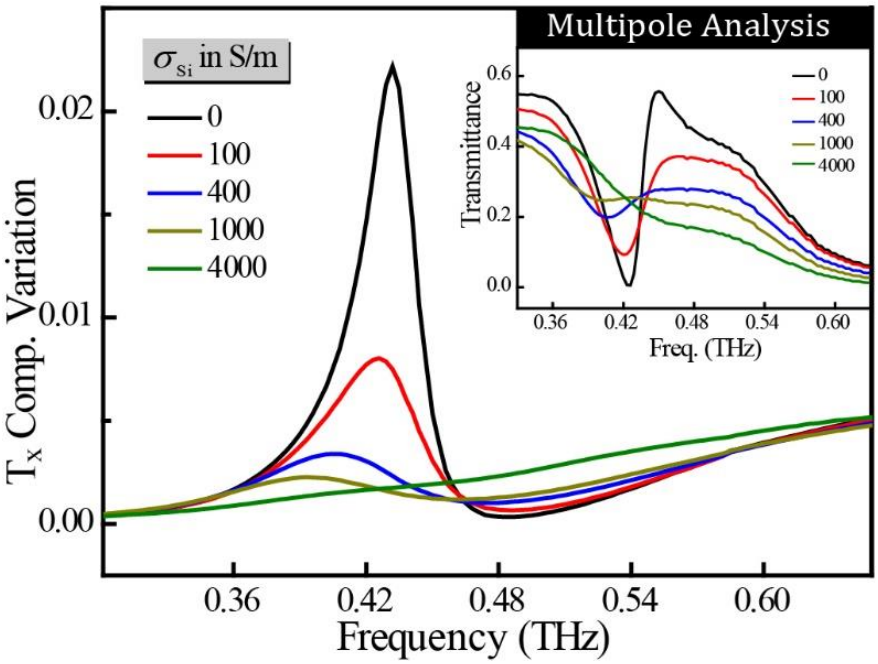

Figure 3. Transmitted intensity (inset plot) and X component of toroidal dipole moment computed through multipole analysis for the increasing conductivity of Si beneath split gaps of TASR.

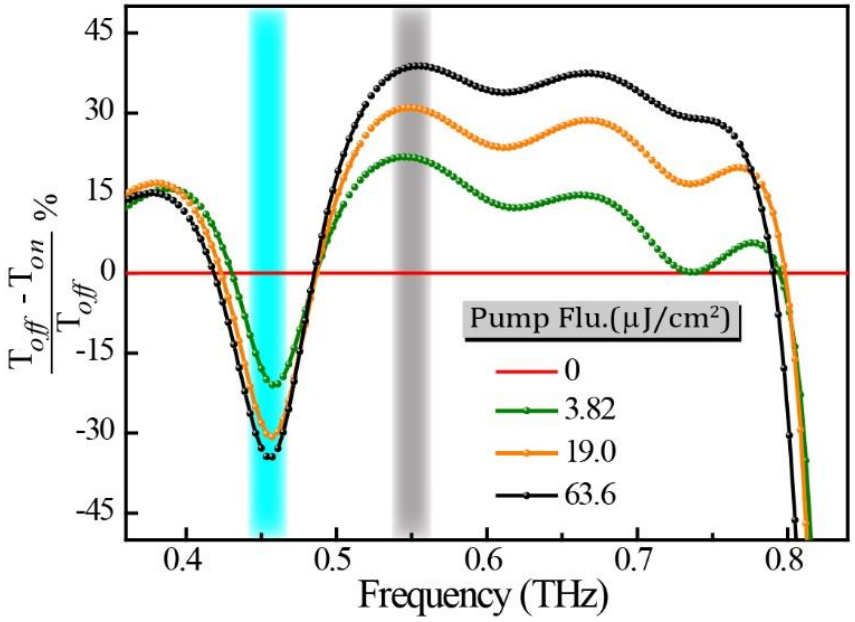

Figure 4. Percentage modulation of experimental transmission amplitude versus frequency plot at different value of the pump fluences. Amplitude modulation ($T_{off} - T_{on}$) at all fluences (0, 3.82, 19.0 and 63.6 μJ/cm^2) has been calculated with respect to corresponding transmission amplitude at zero pump fluence ($T_{off} \rightarrow 0$ μJ/cm^2). Region near resonance depth and transmission peak have been shaded in blue and grey colour, respectively.

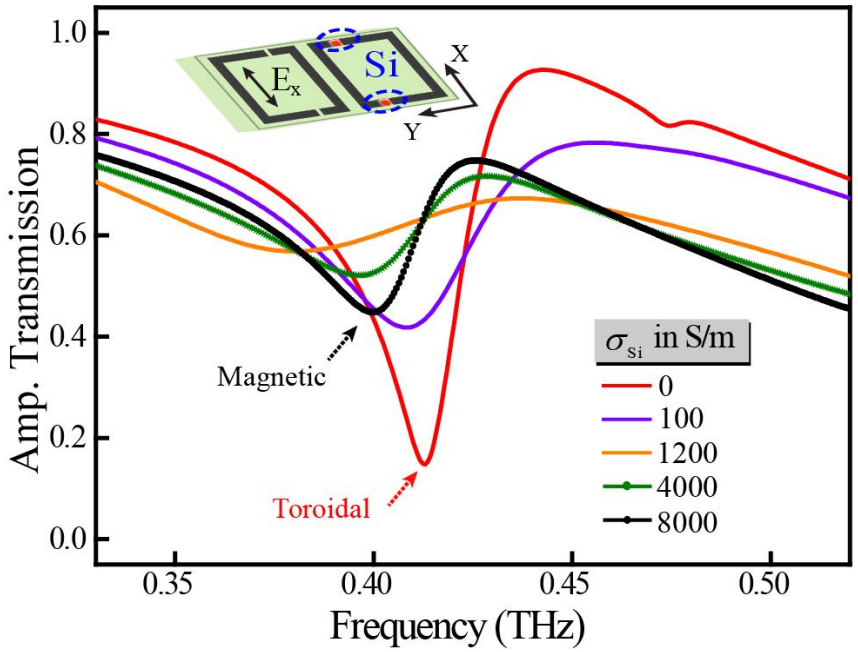

Figure 5. Simulated amplitude transmission versus frequency plot at different conductivities of Si pads lying below the split gaps of only one TASR in mirrored configuration.

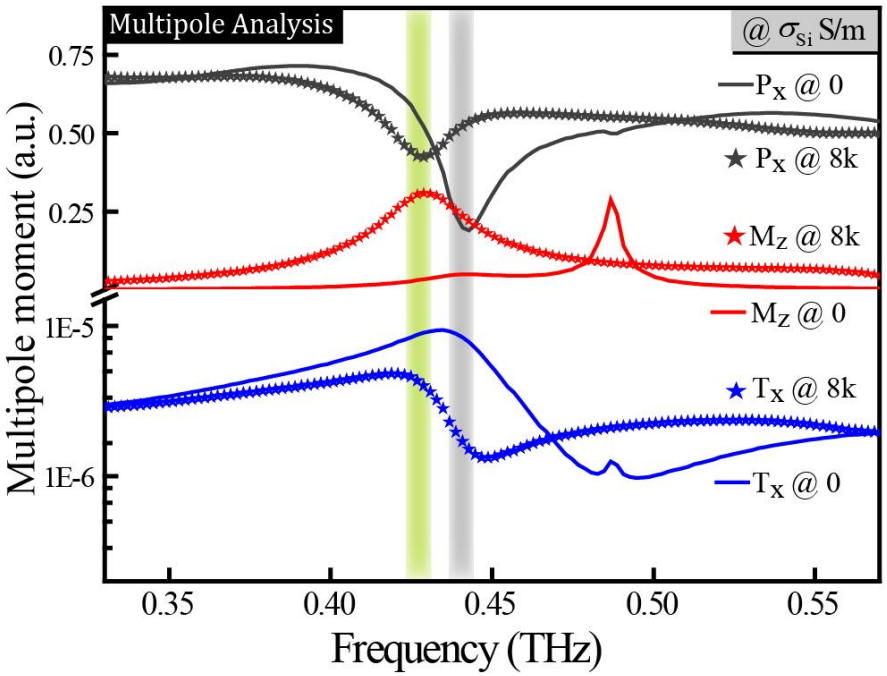

Figure 6. Numerically calculated contribution of electric (P_x) , magnetic (M_z) and toroidal (T_x) dipole moments at two different conductivities (σ_{Si} = 0 and 8000 S/m) of silicon pads lying below the split gaps of only one TASR in mirrored configuration. Shaded region represents the toroidal (grey region) and magnetic (green region) resonance.

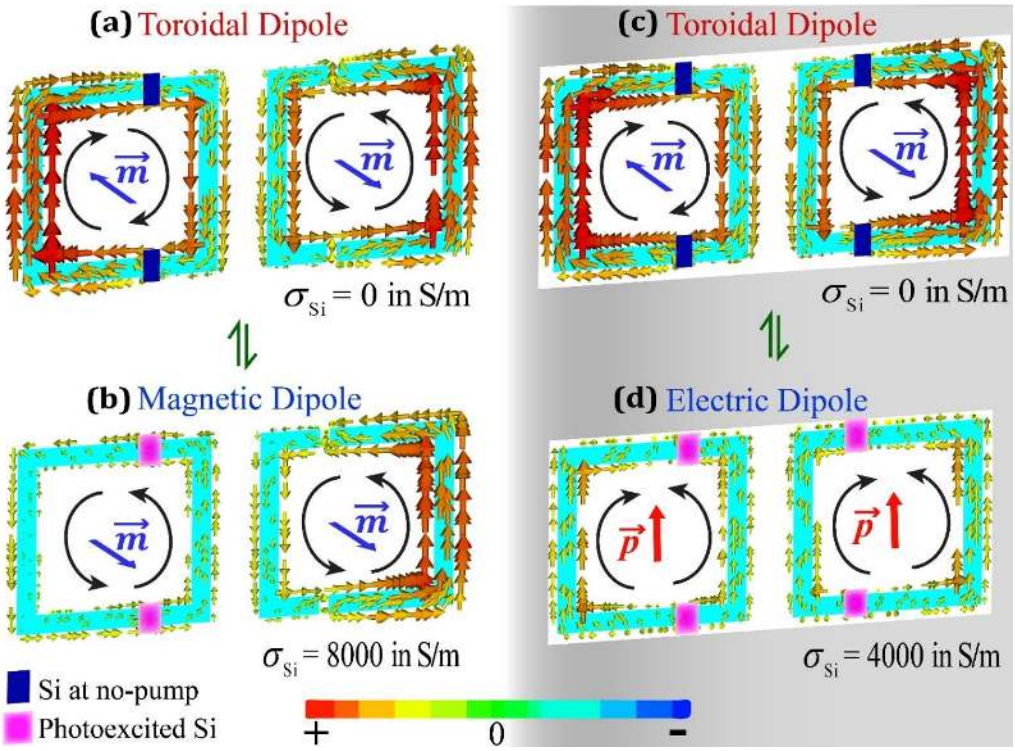

Figure 7. (a, b) Simulated surface currents at 0 and 8000 S/m conductivity of silicon pads lying below the split gaps of only one TASR in mirrored configuration. (c, d) Surface current distribution at 0 and 4000 S/m conductivity of Si pads lying below the split gaps of both TASR in mirrored configuration. Here $\vec{p}$ and $\vec{m}$ denote electric and magnetic dipole moments, respectively.

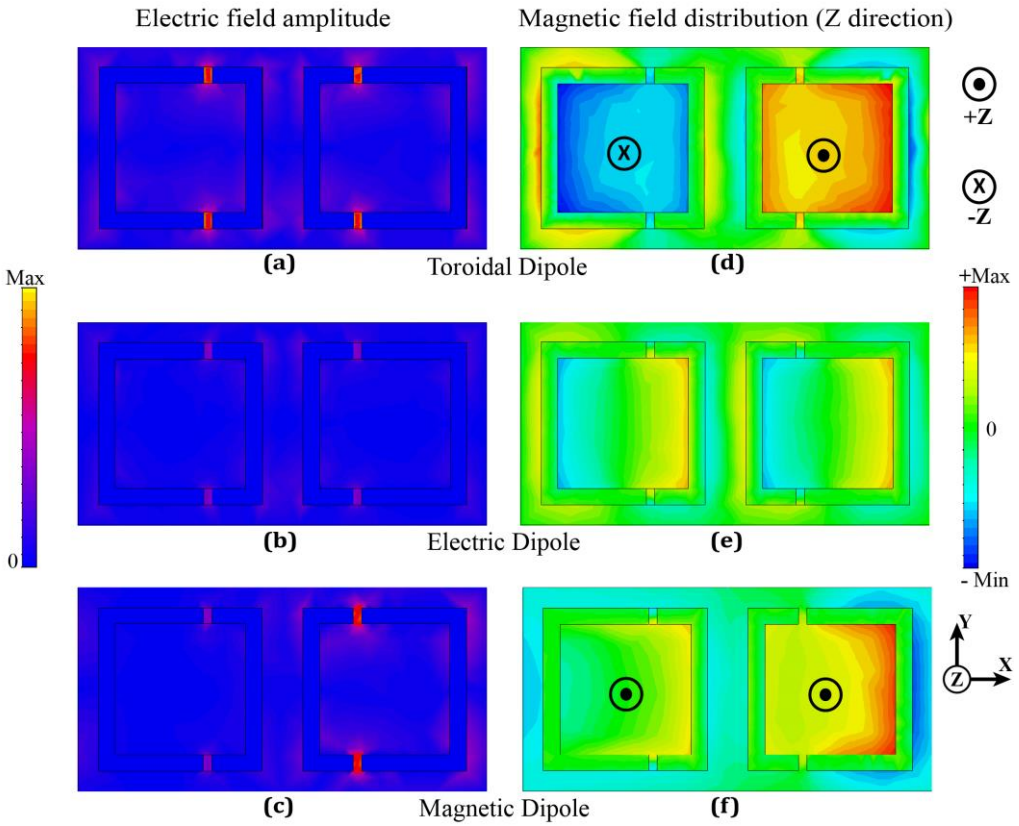

Figure 8. Simulated electric field amplitude (a, b, c) confined in the split gaps of mirrored TASRs and magnetic field distribution (d, e, f) inside coupled TASRs along the Z-direction, as electromagnetic excitation of mirrored TASRs switches from toroidal dipole (a, d) to electric dipole (b, e) or magnetic (c, f) dipole.